Fast Neutron Resonance Radiography for Elemental Imaging: Theory and Applications

Gongyin Chen and Richard C. Lanza, *Member, IEEE*

***Abstract*—Fast neutron resonance radiography (NRR) has been devised as an elemental imaging method with applications such as contraband detection and mineral analysis. In NRR, a two-dimensional (2-D) elemental mapping of hydrogen, carbon, nitrogen, oxygen, and the sum of other elements is obtained from fast neutron radiographic images, taken at different neutron energies and chosen to cover the resonance cross-section features of one or more elements. Images are formed using a lens-coupled plastic scintillator charged coupled device (CCD) combination. In preliminary experiments, we have produced NRR images of various simulants using a variable energy beam based on the Li(p,n)Be reaction and a variable energy proton beam. As an alternative to this method, we have studied NRR imaging using the D-D reaction, d(d,He)n, at fixed incident D energy and scanning through various neutron energies by using the angular variation in neutron energy. The object and detector rotate together around the neutron source; different energy (2–6 MeV) neutrons can be obtained at different angles from the target. The radiographic transmission image provides a 2-D mapping of the sum of elemental contents (weighted by the attenuation coefficients). Transmission measurements taken at different neutron energies (angles) then form a set of linear equations, which can then be solved to map individual elemental contents.**

***Index Terms*—Contraband detection, elemental imaging explosive detection, fast neutron radiography, neutron imaging, resonance radiography, security.**

I. High–Energy Neutron Radiography

FAST neutron radiography with neutron energies of more than 1 MeV opens up a new range of possibilities for nondestructive inspection. One aspect of high-energy neutron radiography is the inspection of objects in the presence of lighter elements. An example of this is in the inspection of such objects as airline luggage or cargo containers. Since most of these objects contain a large amount of hydrogenous materials such as plastics, thermal neutrons are essentially unusable since they are so rapidly moderated by such an environment.

When high-energy neutrons are used for radiography, they are often generated by small accelerators without any moderation. As a result, the beam is kinematically collimated and has a small spot size, making it a more efficient system from the point of view of the neutronics. In practical cases, shielding is a major concern and the geometrical collimation is an important factor in reducing the size of the shielding required for radiation protection.

Manuscript received November 25, 2001; revised March 29, 2002. This work was supported in part by the Office of National Drug Control Policy under Contract DAAD07-98-C-0117, by the Federal Aviation Administration through Grant 93-G-053 and Contract B503612 with Lawrence Livermore National Laboratory.

G. Chen was with the Nuclear Engineering Department, Massachusetts Institute of Technology, Cambridge, MA 02139 USA. He is now with L-3 Security and Detection Systems, Woburn, MA 01801 USA (e-mail: gongyin@alum.mit.edu).

R. C. Lanza is with the Nuclear Engineering Department, Massachusetts Institute of Technology, Cambridge, MA 02139 USA (e-mail: lanza@mit.edu).

Digital Object Identifier 10.1109/TNS.2002.801696

II. Neutron Resonance Radiography

Neutron resonance radiography (NRR) utilizes the element specific resonances in total attenuation cross sections that are in the 1–8 MeV range and that are exploited to enhance the contrast for imaging light elements such as carbon, oxygen, and nitrogen. The goal of this work is to utilize this contrast enhancement mechanism to produce elementally resolved images of objects under inspection.

This work was originally motivated by the need to develop methods for nondestructive inspection for the detection of explosives and other contraband in baggage and cargo [1]–[3]. Other groups have used similar principles and applied them to problems in the minerals industry [4].

III. Fundamentals of NRR

The basic idea of fast NRR is shown in Fig. 1. With a monoenergetic neutron source, we can map one element at a time. We look for an energy region with a resonance peak/valley for one element, while the cross sections of other elements are flat over the same energy range. For example, we might choose the sharp resonance peak at 2.077 MeV for carbon. A radiographic image is taken on-resonance and another taken off-resonance. The difference of the two images gives a two-dimensional (2-D) map of the corresponding element. If only carbon is to be imaged, the broad peak in the 7–8 MeV range is more useful since the width of the peak is so much larger.

Fast NRR with single peaks has low sensitivity when multiple elements are to be detected and faces some practical difficulties, which will be discussed in more detail later. We will show a straightforward method to use neutrons of wide-energy spectrum and to exploit the broad resonance features of elements of interest.

A radiographic image is a 2-D map of projected attenuation and can also be thought of as a 2-D map of the sum of the contents of all existing elements, weighted by their attenuation coefficients. For each pixel in the image, there exists a linear equation stating that the total attenuation equals the weighted sum of projected elemental contents. When we take another radiographic image with a different energy spectrum, the resulting linear equations have different attenuation coefficients

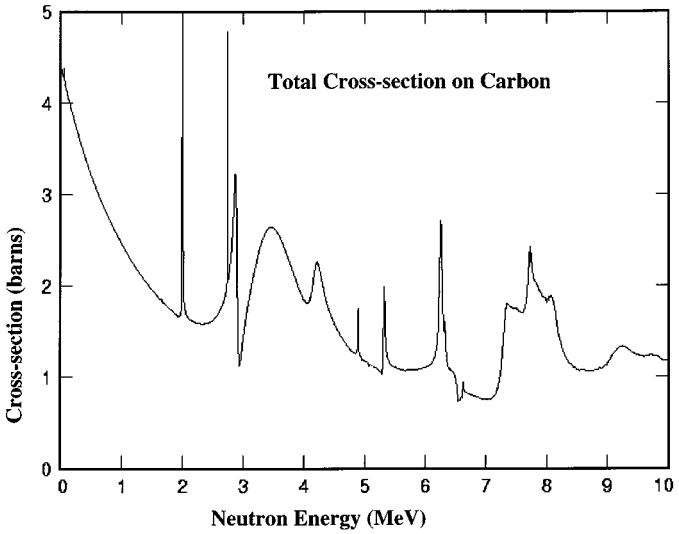

Fig. 1. Resonance radiography with a single peak.

(weighting factors or attenuation coefficients) and total attenuation, but have the same projected contents, as the object is the same. In principle, when there are more equations than the number of existing elements, the set of linear equations can be solved as a definite least-squares solution for the projected elemental contents [5]. A typical fast neutron radiography setup is shown in Fig. 2 [6].

IV. Fast Neutron Production

The most common way of producing fast neutrons for radiography is through nuclear reactions, which requires a particle accelerator and a target. A p-^{7}Li source and a D-D source were used in our study. The former source involves two nuclear reactions and the latter has only one reaction channel

$$^7\mathrm{Li} + p = {}^7\mathrm{Be} + n - 1.646\ \mathrm{MeV} \quad (1)$$

$$^7\mathrm{Li} + p = {}^7\mathrm{Be}^* + n - 2.076\ \mathrm{MeV} \quad (2)$$

$$^2\mathrm{H} + d = {}^3\mathrm{He} + n + 3.27\ \mathrm{MeV}. \quad (3)$$

The p-^{7}Li source has slower energy falloff than the D-D source, so it is a better mono-energetic neutron source for imaging applications (see Fig. 3). With energy falling off at increasing angle, different parts of the image experience different energy neutrons. This is important if the imaging method requires mono-energetic neutrons such as NRR with single peaks. The applicable angles beyond which the object should not extent are 10° and 5° for both sources, respectively. In addition, the p-^{7}Li source is usually contaminated with gamma rays while the D-D source is generally not.

V. Image Recording

A straightforward way of doing neutron resonance radiography is to map one element at a time. At an energy region with a resonance peak or valley for one element (while the cross sections of other elements are flat over the same energy range), we take a radiographic images at on-resonance energy and an off-resonance energy and then compute the pixel-by-pixel difference of the two images.

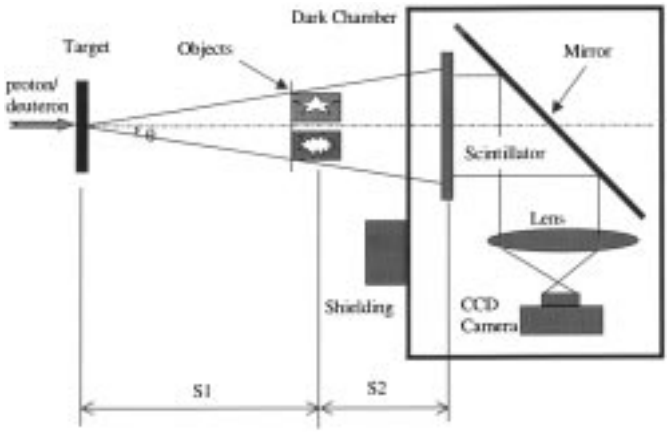

Fig. 2. Fast neutron radiography hardware.

The 1.5–2.5 MeV region is suitable for this purpose. Fig. 4 shows the peaks used for three different elements. Unfortunately, hydrogen has no resonance peak.

Initial experiments were run with single peak NRR. A p-^{7}Li neutron source was used, with a 2–6 MeV proton beam from the University of Massachusetts at Lowell Van de Graaff accelerator. Neutron yield was about 5×10^7 neutrons/sr/s at 0° with typical proton currents of 5–10 μA. Since resonance peaks are typically 10–30 keV in width, a thin target was required for mono-energetic neutron generation.

Using the camera system of Figs. 2, 5 shows images taken of a series of test objects: drug simulant (top left), explosive simulant (bottom left), graphite powder (top right) and melamine (bottom right), in 35 mm photographic film containers. The axes are in units of pixels, each pixel is about 0.5 mm. Source-object distance was $\sim$ 30 cm and object-detector distance was $\sim$ 15 cm. The objects are within a 10° beam cone. ($S1 = \sim 30$ cm, $S2 = \sim 15$ cm, $\theta < 10°$)

The simple method employed here has several significant problems in practical applications. First, we note that single distinct resonance peaks are usually found in the 1.5–2.5 MeV neutron energy region, where the total neutron cross section (especially that of hydrogen) is large and, therefore, neutron penetration is poor. Second, since the resonance peaks are 10–30 keV in width, this requires a thin target to maintain a beam of essentially mono-energetic neutrons. A small viewing angle ($\theta < 10°$) is required so that the neutron energy falloff across the image is significantly smaller than the difference between on and off resonance energy. Finally, different energy neutrons are obtained by changing the accelerator energy, an undesirable requirement in inspection applications where high throughput is required. For some applications where only a single element is being detected, the single-peak approach is considerably more practical [4]. This particular implementation has practical limitations but is useful to demonstrate the technique.

In the presence of more elements, it becomes difficult to find distinct resonance peaks for all elements of interest. In addition, neutron resonance radiography with distinct resonance peaks suffers from the practical problems discussed in the previous paragraph. To improve the method, we investigated through simulation the broad resonance structure at neutron energies of 2–6 MeV and show how neutron resonance radiography with

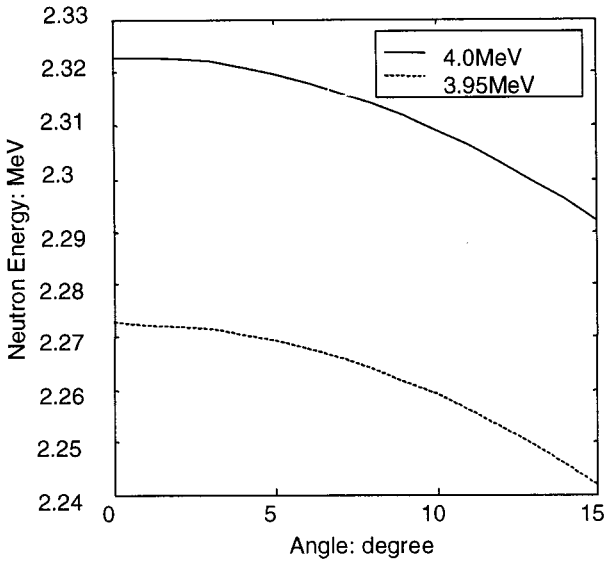

(a) (b)

Fig. 3. Energy falloff of (a) p-^{7}Li and (b) D-D.

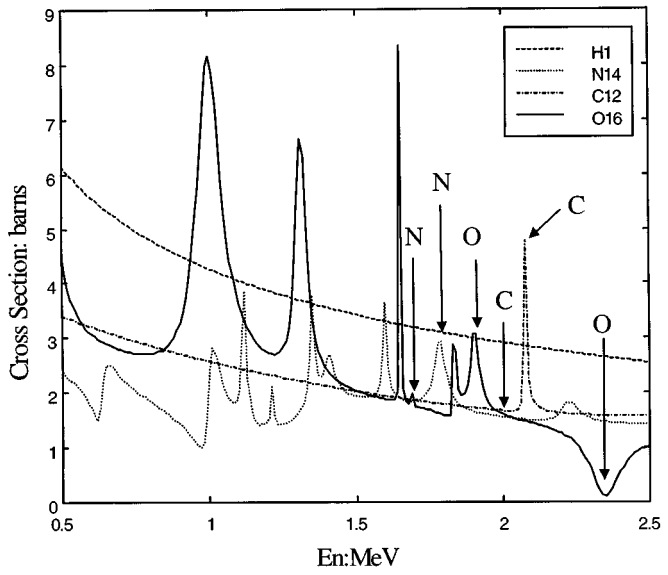

Fig. 4. Single peaks chosen for resonance radiography.

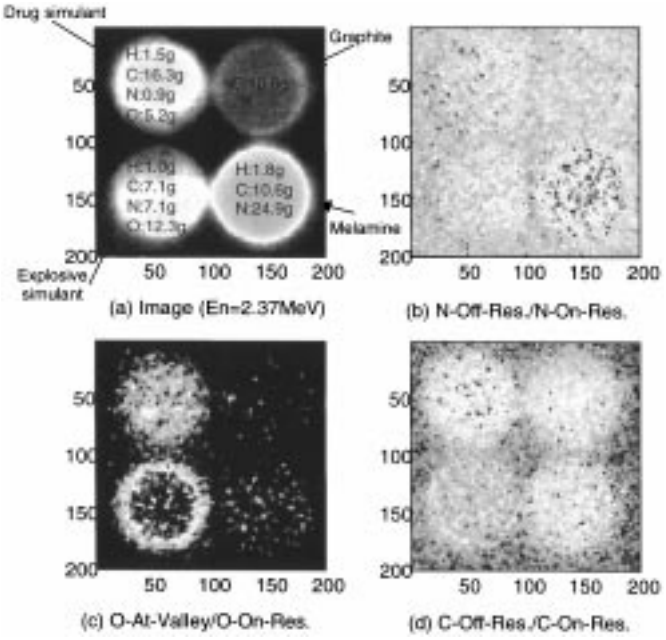

Fig. 5. NRR with single peaks. (a) Image at 2.37 MeV. (b) Nitrogen on and off resonance. (c) Oxygen on and off resonance. (d) Carbon on and off resonance.

broad peaks can be made practical. For example, we can take m radiographic image at m energy bins for the bulk material composed of n elements and we obtain the following equations for *each* pixel over the image:

$$\begin{aligned}
a_{11}x_1 + a_{12}x_2 + a_{13}x_3 + \cdots + a_{1j}x_j + \cdots + a_{1n}x_n &= b_1 \\
a_{21}x_1 + a_{22}x_2 + a_{23}x_3 + \cdots + a_{2j}x_j + \cdots + a_{2n}x_n &= b_2 \\
\cdots\cdots\cdots\cdots\cdots\cdots\cdots\cdots & \\
a_{i1}x_1 + a_{i2}x_2 + a_{i3}x_3 + \cdots + a_{ij}x_j + \cdots + a_{in}x_n &= b_i \\
\cdots\cdots\cdots\cdots\cdots\cdots\cdots\cdots & \\
a_{m1}x_1 + a_{m2}x_2 + a_{m3}x_3 + \cdots + a_{mj}x_j + \cdots + a_{mn}x_n &= b_m
\end{aligned} \tag{4}$$

where the a_{ij} are the attenuation coefficients, the x_j are the projected elemental contents and the b_i are the measured total attenuations. The (over-determined) equation set can be solved to map elemental contents.

We pick an energy bin that contains resonance feature of one or more elements and take a radiograph. Each element attenuates neutrons as if there were only this single element in the path and the total attenuation is the sum of attenuation by all elements present. The resulting equation shows that the total attenuation is the sum of attenuation by all elements is not sufficient to tell us the contents of any element. In order to do this, we take radiographic images at more energy bins and obtain more similar equations. The method is analogous to spectral

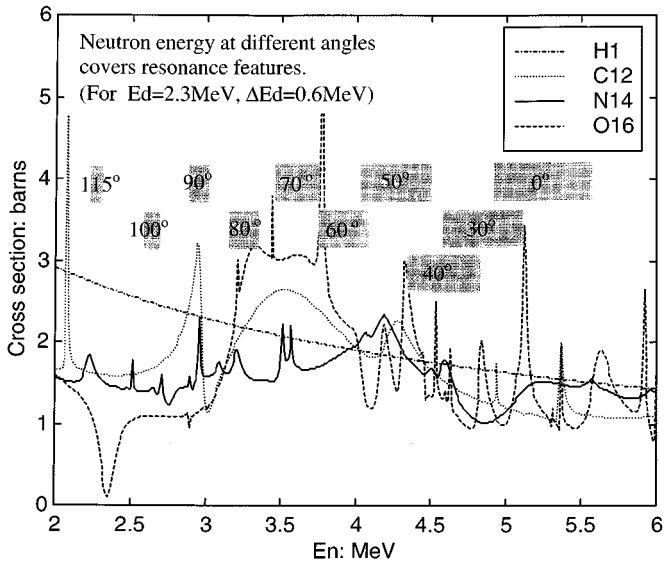

Fig. 6. Desired energy bins for NRR.

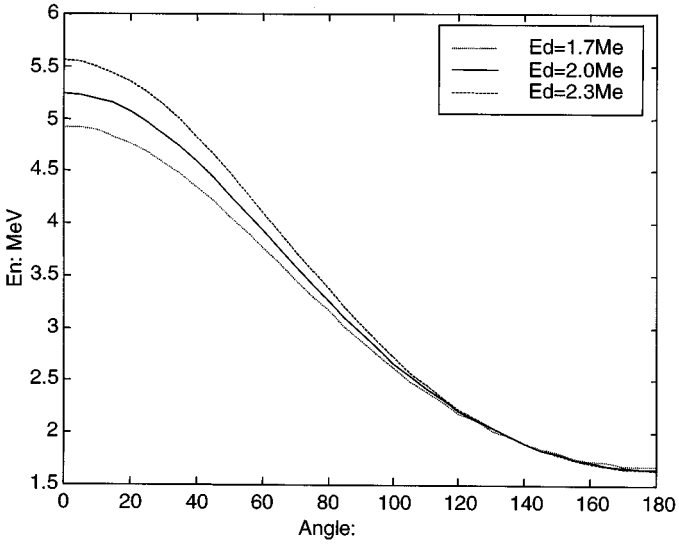

Fig. 7. D-D neutron energy as a function of angle.

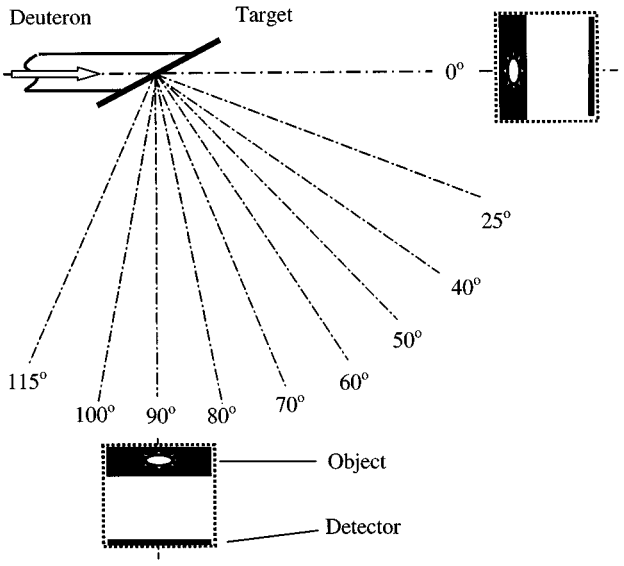

Fig. 8. Rotational geometry.

fitting methods for determining elemental composition through gamma spectroscopy where detectors with relatively poor spectral resolution are used, but the resulting spectrum is fitted to a series of low-resolution spectra from individual elements. The desired energy bins for [H, C, N, and O] imaging are shown in Fig. 6.

A practical concern is how we can obtain neutrons of different energy. The neutron energy from a D-D source has a strong angular dependence (Fig. 7), which can be used to obtain the desired neutron energies (Fig. 6) by introducing a simple rotational geometry (Fig. 8).

Fast neutrons for resonance radiography are generated by bombarding a deuteron target with energetic deuterons accelerated by a fixed energy RF quadrupole (RFQ) accelerator. The major advantage of the RFQ is that it is very compact and capable of high-current operation. The usual disadvantage of an RFQ, fixed energy, is not a disadvantage in this application since we use the angular dependence of the neutron energy to vary energy. The choice of target is flexible. If the current is low ($\sim$ 10 μA) and the beam spot a diameter of $\sim$ 1 cm, then thin pressure windows can be used. Various approaches have been made to overcome the thermal and mechanical problems of thin windows, generally by the use of windowless targets [7], [8]. We have assumed in our design studies 6 atm-cm of gas at a pressure of 3 atm.

VI. Security Applications

A series of radiographic images were simulated with different neutron spectra, as obtained from different angles of a D-D neutron source. The attenuation coefficients were also simulated with these neutron spectra for elements of interest such as hydrogen, carbon, nitrogen, and oxygen. A constant attenuation coefficient (2.5×10^{-24} cm^2) was used for the fifth component, which represents all other elements. Elemental images were calculated for each pixel from the attenuation coefficients and radiographs, using the linear equations.

The object modeled in the simulations is a "terrorist overnight bag" [10]. The bag itself consists of a thin aluminum shell ($\sim 40 \times 30 \times 10$ cm^3) with a wood handle, thick cloth covering, and steel fittings. It contains a newspaper, a bag of sugar ($\sim$ 100 g), cocaine-HCl ($\sim$ 100 g), a travel umbrella, a 4-in switchblade knife, a paperback book (presumably the *Anarchist's Handbook*), a 300-g block of plastic explosive (50/50 wt.% mix of RDX and PETN), a pen and pencil set, a small camera, an automatic pistol with extra ammunition clip, a flat paper notebook, and a selection of cotton, wool, and nylon clothing items. The bag is heavily loaded with an average density of $\sim$ 0.5 g/cm^3. Fig. 9 gives the simulated neutron image at 0° (left) and 140-keV X-ray image (right).

Neither method tells the book from the plastic explosive or the sugar bag from the drug bag. After more neutron images are taken, elemental images are calculated by solving an equation set for each pixel and an image is generated as in Fig. 10. With NRR results, we know the elemental composition of items as

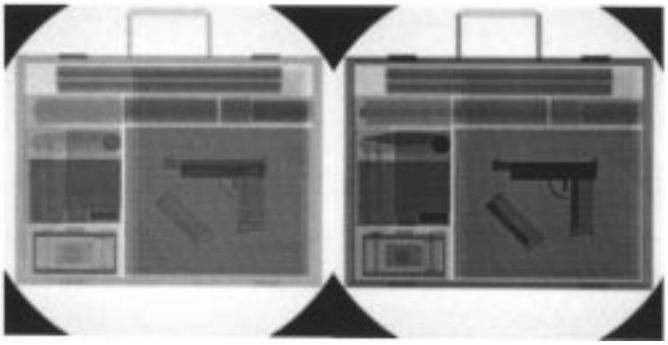

(a) (b)

Fig. 9. Fast neutron radiograph at (a) 0° and (b) X-ray radiograph.

well as their shapes, which makes it possible to distinguish between organic materials of similar density. The plastic explosive can be identified by its high nitrogen and oxygen content and low hydrogen and carbon content. The cocaine looks different from sugar in that the drug has about equal amounts of hydrogen and carbon but very little oxygen. The bright bar overlapping the drug bag in the carbon image is the polystyrene handle of an umbrella. The pistol, knife blade, and the battery are visible in the "other" picture. A glass lens in the camera is also very clear in the oxygen picture. Two aluminum buckles can be seen on the top in the hydrogen picture. As we have mentioned, the calculation splits aluminum content into hydrogen and "other" results. Although our primary interest is in drug and explosive detection, the NRR principle is clearly not restricted to such systems provided suitable resonance energies are found.

A practical design for such a system would use a 2.3-MeV RFQ deuteron accelerator and a deuterium target. With a 2-cm-long target at 3 atm, we estimate that a practical neutron flux can be achieved with 10 μA or more average deuteron current.

VII. Shielding Considerations

An important part of any deployable neutron system is the ability to shield the system for radiological safety [11]. A possible design of source shielding for a D-D source (2×10^9 neutrons/s) is shown in Figs. 11 and 12. It consists of an ellipsoidal polyethylene shield with a lead covering. Since only a small fraction of the neutrons will be used for imaging, the initial shielding has two apertures on the side. Most of the neutrons are removed close to the source in order to reduce background in the imaging and also to reduce the shielding required behind the imaging station. The radiation dose equivalent at the surface of the source shielding is higher than the allowed 2.5 mrem/h limit, but if we enclose the $R = 120$ cm region (centered at the source point, not the shielding structure center), the dose outside the enclosure is below 2 mrem/h and meets National Council on Radiation Protection (NCRP) standards. The 120-cm distance is allowed by the imaging geometry (source-object distance 1.5 m or 2 m). The calculated dose at 120 cm from the source is shown in Fig. 13. Note that, as expected, the maximum neutron dose is in the forward direction, which simplifies the shielding of a practical system.

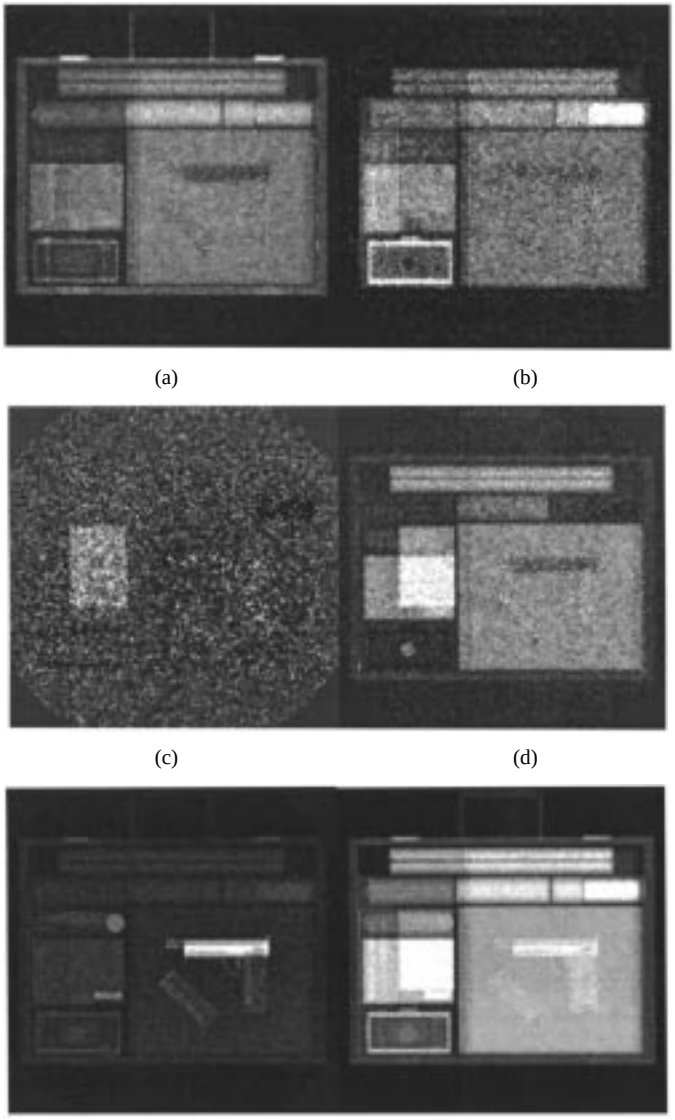

(a) (b)

(c) (d)

(e) (f)

Fig. 10. Calculated elemental images for different elements: (a) hydrogen; (b) carbon; (c) nitrogen; (d) oxygen; (e): other; and (f) all elements.

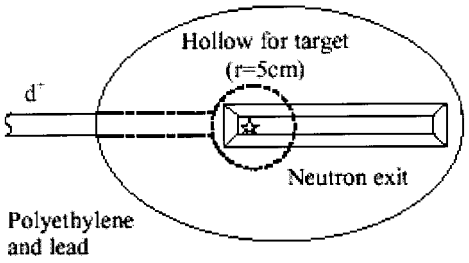

Fig. 11. Side view of shielding showing aperture for neutron beams.

VIII. Conclusion

Neutron resonance radiography provides a method for obtaining both elemental composition of objects under inspection as well as high resolution ($\sim$ mm) imaging. The spatial resolution is not as good as X-ray systems but, unlike X-ray systems, elemental composition and density are measured. The limits on resolution are established mostly by the size of the beam and

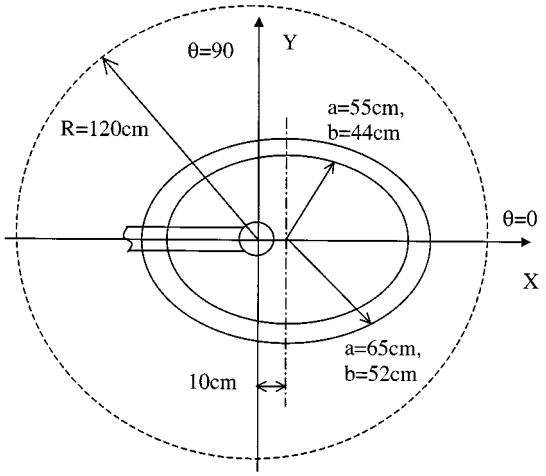

Fig. 12. Source shielding.

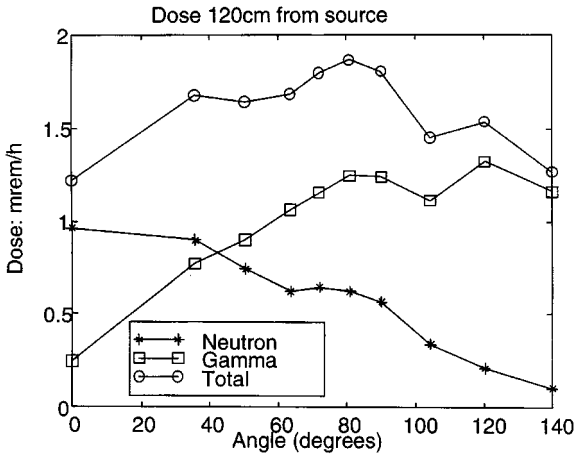

Fig. 13. Dose in mrem/h at 120 cm from 2×10^9 n/s source.

the resolution of the detector. The most important aspect of this technique, the determination of elemental composition provides an extremely powerful method for identification of threat materials, which more than compensates for the lower spatial resolution. As we have mentioned, the beam size is determined by limitations in the power handling of conventional windowed gas targets; the use of windowless targets, while somewhat more complex can be used to obtain mm resolution images. New developments in imaging detectors may enable spatial resolution comparable to X-rays and, in principle, the technique can be expanded to tomographic imaging as well.

ACKNOWLEDGMENT

The authors would like to thank J. Hall, Lawrence Livermore National Laboratory, Livermore, CA, for his help in simulations and in the physics of fast neutron radiography. They would also like to thank R. Ambrosi and J. Watterson, University of Witwatersrand, Johannesburg, South Africa, and J. Guzek and S. Tapper, deBeers, Johannesburg, South Africa, for many useful discussions and ideas.

REFERENCES

[1] "National Drug Control Strategy: 2000 Annu. Rep.," Executive Office of the President, Office Nat. Drug Contr. Policy, 2000.

[2] G. Chen, "Fast neutron resonance radiography for elemental imaging: Theory and applications,", Ph.D. dissertation, Dept. Nucl. Eng., Massachusetts Inst. Technol., 2001.

[3] *Proc. 1st Int. Symp. Explosive Detection Technology*, Atlantic City, NJ, Nov. 1991.

[4] J. Guzek, "Elemental radiography using fast neutron beams,", Doctor of Philosophy dissertation, Univ. Witwatersrand, Witwatersrand, South Africa, Dec. 1999.

[5] G. Chen and R. C. Lanza, "Neutron resonance radiography (NRR) for security applications," in *Proc. 16th Int. Conf. Application of Accelerators in Research and Industry*, vol. 576, AIP Conf. Proc., J. L. Duggan and L. I. Morgan, Eds., New York, 2001, pp. 1109–1112.

[6] R. C. Lanza, S. Shi, and E. W. McFarland, "A cooled CCD-based neutron imaging system for low fluence neutron sources," *IEEE Trans. Nucl. Sci.*, vol. 43, pp. 1347–1351, June 1996.

[7] J. Guzek, K. Richardson, C. B. Franklyn, A. Waites, W. R. McMurray, J. I. W. Watterson, and U. A. S. Tapper, "Development of high pressure deuterium gas targets for the generation of intense mono-energetic fast neutron beams," *Nucl. Instrum. Methods*, vol. B152, no. 4, pp. 515–526, 1999.

[8] A. de Beer, A. Hershcovitch, C. B. Franklyn, S. van Straaten, and J. Guzek, "Performance of a plasma window for a high pressure differentially pumped deuterium gas target for mono-energetic fast neutron production-preliminary results," *Nucl. Instrum. Methods*, vol. B170, pp. 259–265, 2000.

[9] J. Hall, F. Dietrich, C. Logan, and G. Schmid, "Development of high-energy neutron imaging for use in NDE applications,", UCRL-JC-134 562, 1999.

[10] J. Hall, "Monte Carlo modeling of neutron and gamma-ray imaging systems," in *Proc. 5th Int. Conf. Applications of Nuclear Techniques*, Crete, Greece, Bellingham, WA: SPIE, pp. 465–468, 1997, G. Vourvopoulos, Ed., June 1996.

[11] "Radiation protection design guidelines for 0.1–100 MeV particle accelerator facilities,", Washington, DC, NCRP Rep. 51, 1977.